# Electronic Supplementary Information

## Modulating the structure of iron-doped titanium nitride deposited on nitrogen-doped carbon catalyst for the oxygen reduction reaction in Zn-air battery

Pengfei Zheng,[ab]† Siqi Hu,[ab]† Lina Han,*[ab] Yidan Fu,[ab] Xiaoyuan Zeng,[b] Mian Li,[b] Jing Feng,[a] Yudong Sui,*[a] Peng Dong,[b] Yingjie Zhang*[ab]

a School of Materials Science and Engineering, Kunming University of Science and Technology, Kunming 650000, P. R. China.

b National and Local Joint Engineering Laboratory for Lithium-ion Batteries and Materials Preparation Technology, School of Kunming University of Science and Technology, Kunming 650000, P. R. China.

† Pengfei Zheng, and Siqi Hu. contributed equally.

* Corresponding Author: Lina Han, Kunming University of Science and Technology, PR China;

Email: hanln2016@163.com.

**Chemicals**

All chemicals were commercially available and used without further purification. Titanium isopropoxide (TTIP, 95%) and Iron sulfate heptahydrate ($FeSO_4 \cdot 7H_2O$, A.R., ≥99%) were purchased from Aladdin reagent. Poly (ethylene glycol)-block-poly (propylene glycol)-block-poly (ethylene glycol) (P123) and Perfluorosulfonic acid-PTFE copolymer (Nafion, 5% w/w solution) were provided from Sigma-Aldrich. Ethanol (≥99.7%,) and Methanol ($CH_3OH$, ≥99.5%) were obtained from Tianjin Fengchuan Chemical Reagent Co., Ltd. Hydrochlochric acid (HCl) was purchased Xilong Science Co., Ltd. Dicyandiamide (DCDA, ≥99.5%,) was provide from Acros. Pt/C (nominally 20% wt.) was purchased from Shanghai Hesen Electric Co., Ltd.

**Characterization**

The Field-emission scanning electron microscopy (FESEM) study was conducted on a FEI Quanta 200 with an operation voltage of 20 kV. Transmission electron microscopy (TEM) and high-resolution TEM (HRTEM) observations were conducted on a Tecnai G2 TF30S-Twin microscope operated at 300 kV. The X-ray diffraction (XRD) was characterized on a Rigaku MiniFlex 600 with a Cu Kα radiation source (λ = 1.5406 Å) at 40 kV. The surface area and pore structure of the catalysts were investigated by the Micromeritics ASAP 2460 Surface Area and Porosity Analyzer at 77 K. Raman spectra were measured on a Renishaw in Via Raman microscope spectrometer at 532 nm. The surface chemical composition was carried out by the Thermo Fisher Scientific K-Alpha+ (Al Kα, 1486.6 eV) XPS spectrometer.

**Calculation of the electron transfer number ($n$)**

The number of electrons transported ($n$) at different potentials was determined by Koutecky-Levich (K-L) plots ($n$ and $j_k$ can be obtained from the slope and intercept of the K-L plots):

$$\frac{1}{j} = \frac{1}{j_k} + \frac{1}{j_L} = \frac{1}{j_k} + \frac{1}{B\omega^{1/2}}$$

$$B = 0.62nFC_{O_2}D_{O_2}^{2/3}v^{-1/6}$$

Where $j$ $j_k$ and $j_L$ are the measured current density, kinetic and diffusion-limiting current densities, respectively, $n$ is the electron transfer number, F is the Faraday constant (96485 C mol$^{-1}$), $\omega$ is the angular velocity, $C_{O_2}$ is the bulk solubility of $O_2$ (ca. $1.2 \times 10^{-6}$ mol cm$^{-3}$ for 0.1 mol L$^{-1}$ KOH), $D_{O_2}$ is the diffusion coefficient of $O_2$ (ca. $1.9 \times 10^{-5}$ cm$^2$ s$^{-1}$ for 0.1 mol L$^{-1}$ KOH), and v is the kinematic viscosity of the electrolyte (0.01 cm$^2$ s$^{-1}$).

**Supplementary Figures and Tables**

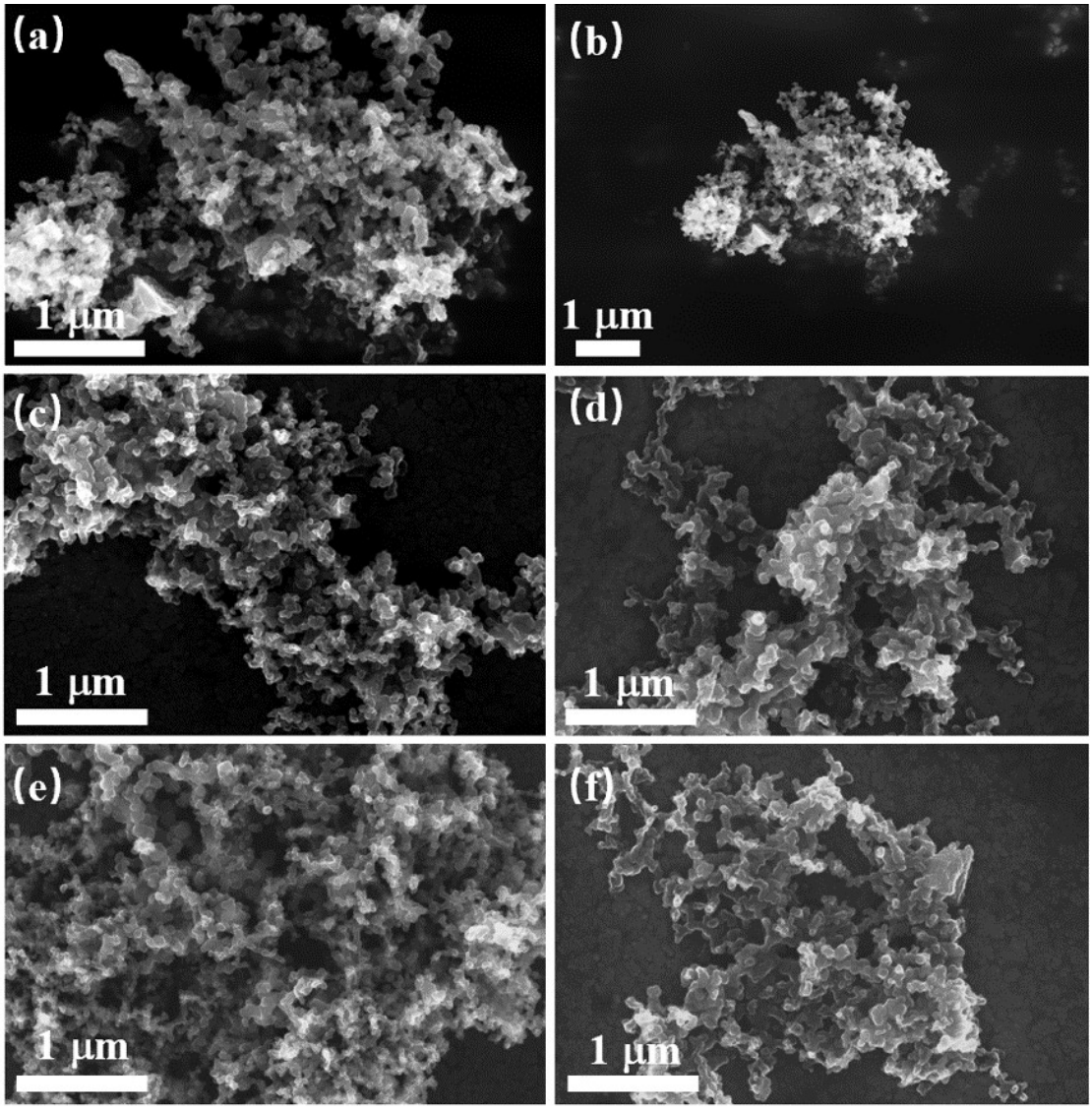


**Figure S1.** The FESEM images of (a,b) TiN/NC/C, (c) $Ti_{0.97}Fe_{0.03}N$/NC/C, (d) $Ti_{0.95}Fe_{0.05}N$/NC/C, (e) $Ti_{0.93}Fe_{0.07}N$/NC/C and (f) $Ti_{0.91}Fe_{0.09}N$/NC/C.

In the as-prepared catalysts, the interconnected spherical structures were well preserved on the $Ti_xFe_{1-x}N$/NC/C catalysts, with no obvious change after the introduction of Fe ions. Furthermore, due to the uniform distribution of the active sites and the distinctive interconnected sphere-like structure, the catalyst possesses efficient mass and charge transport during the ORR process.

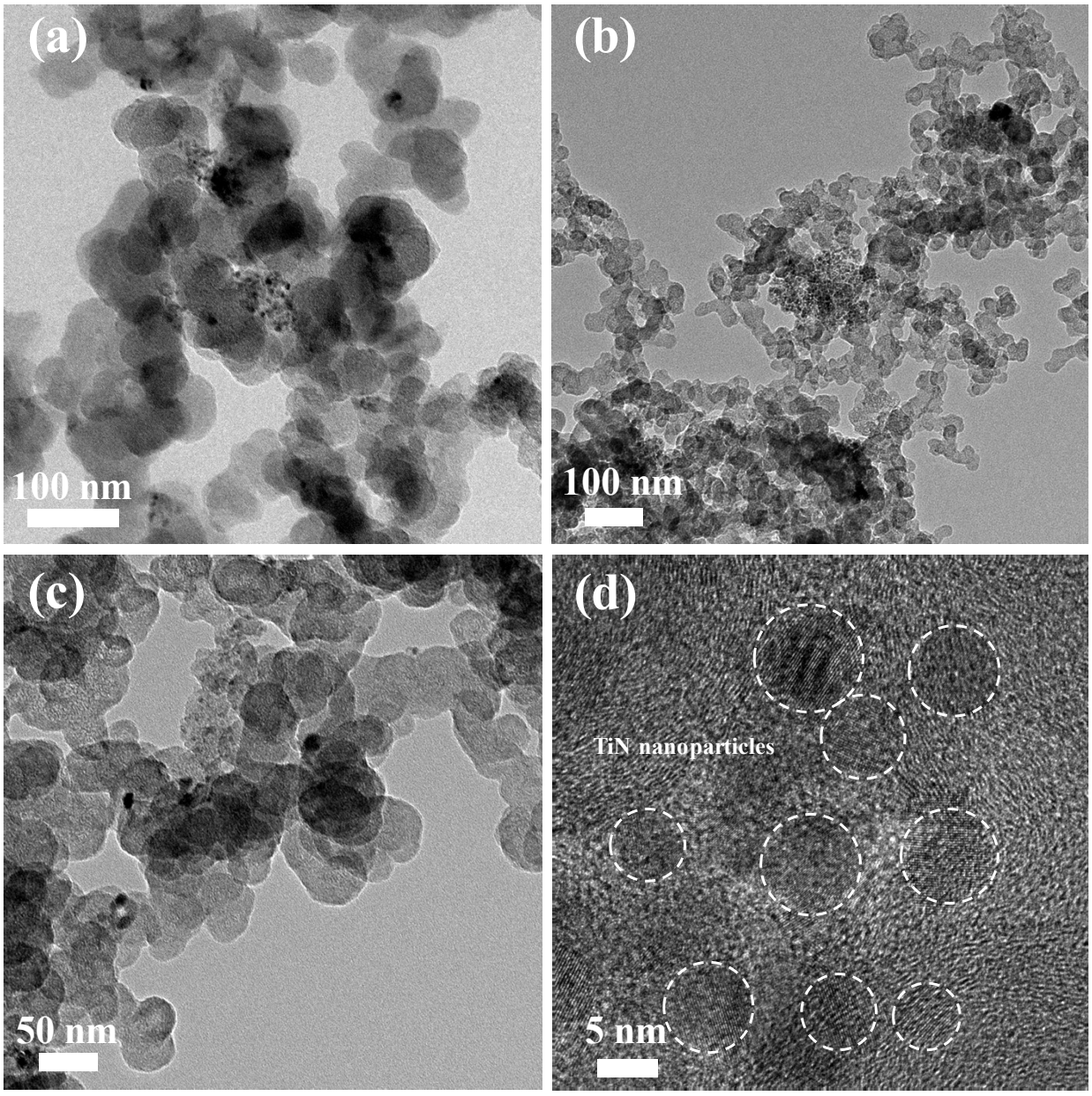


**Figure S2.** (a-d) The TEM and HRTEM images of TiN/NC/C

The detailed structural information of the obtained TiN/NC/C samples was further characterized by TEM at different magnifications. With a particle size of around 36 nm, interconnected TiN spherical nanoparticles were found to be equally diffused. Clear lattice fringes can be seen in the HRTEM image, and the measured lattice spacing of 0.215 nm is in accordance

with the (2 0 0) plane of TiN.

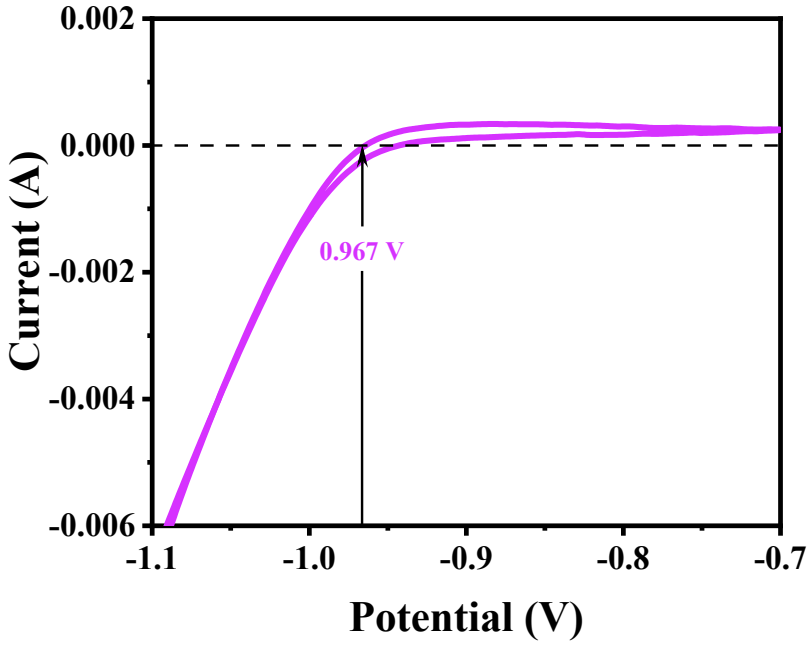


**Figure S3.** Cyclic voltammetry in an $H_2$-saturated 0.1 M KOH electrolyte at a scan rate of 0.2 mV $s^{-1}$ to calibrate a reversible hydrogen electrode (RHE).

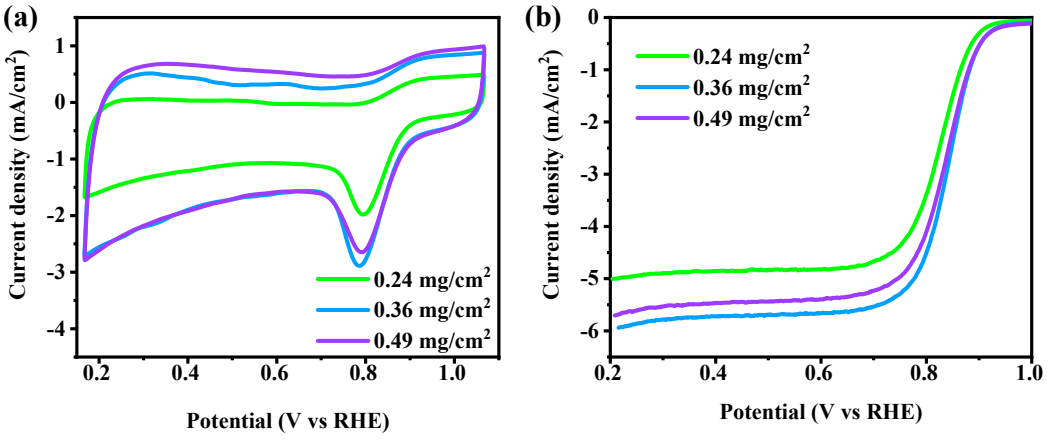


**Figure S4.** (a) CV and (b) LSV diagrams in $O_2$-saturated 0.1M KOH solution of $Ti_{0.95}Fe_{0.05}N$/NC/C with different loadings.

Using $Ti_{0.95}Fe_{0.05}N/NC/C$ as an example, we discovered that when the loading was 0.36 mg·cm$^{-2}$, the oxygen redox peak of the CV is more obvious in the Figure S3a, and shown in the Figure S3b of the LSV plot, the half-wave potential and limit current were 0.83 V and 5.96 mA·cm$^{-2}$, respectively. But that if the loading was increased to 0.49 mA·cm$^{-2}$, the limit current decreased, so we decided that all catalyst loading in this paper would be 0.36 mg·cm$^{-2}$.

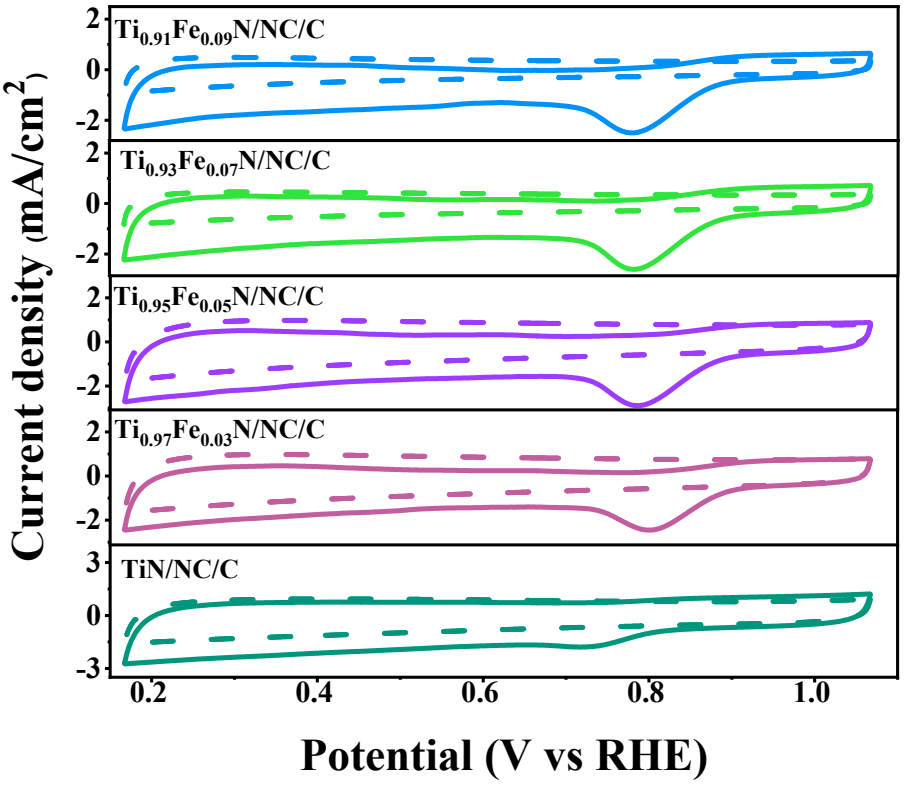


**Figure S5.** CV curves of the TiN/NC/C, $Ti_{0.97}Fe_{0.03}N/NC/C$, $Ti_{0.95}Fe_{0.05}N/NC/C$, $Ti_{0.93}Fe_{0.07}N/NC/C$ and $Ti_{0.91}Fe_{0.09}N/NC/C$ in $O_2$-saturated and $N_2$-saturated 0.1M KOH solutions.

As shown in the Figure S4, the CV curves shows a distinct oxygen redox peak in an $O_2$-saturated 0.1M KOH electrolyte, revealing that a distinct ORR activity for all the as-made catalyst. It's worth

noticing that $Ti_{0.95}Fe_{0.05}N/NC/C$ possesses a more positive potential than the other catalysts, implying that it has superior oxygen reduction catalytic activity.

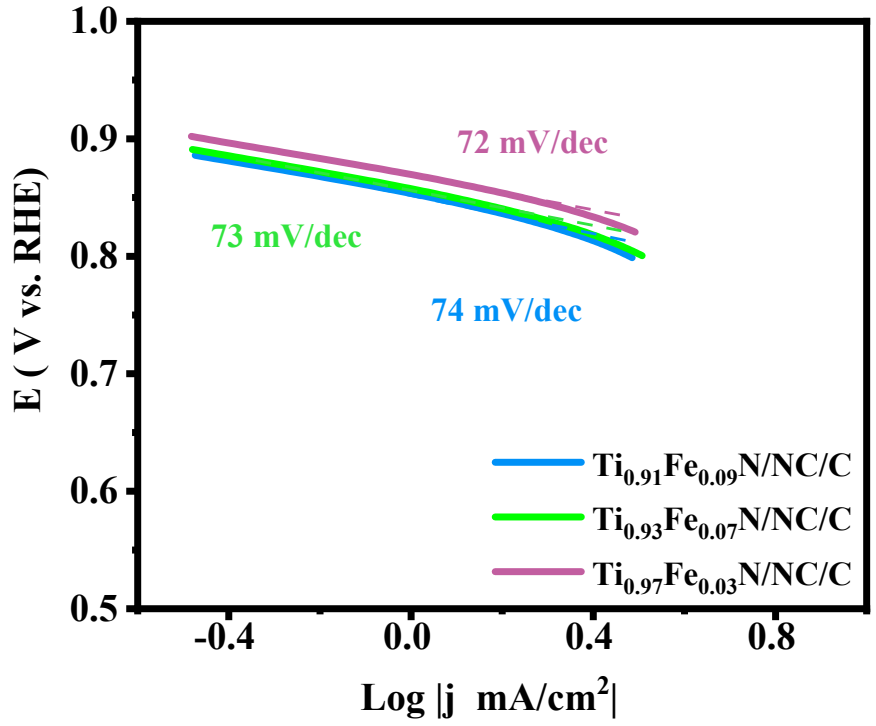


**Figure S6.** ORR Tafel slops obtained from the LSV plots of $Ti_{0.91}Fe_{0.09}N/NC/C$, $Ti_{0.93}Fe_{0.07}N/NC/C$ and $Ti_{0.97}Fe_{0.03}N/NC/C$.

According to the ORR, the corresponding Tafel slops of $Ti_{0.91}Fe_{0.09}N/NC/C$, $Ti_{0.93}Fe_{0.07}N/NC/C$, and $Ti_{0.97}Fe_{0.03}N/NC/C$ are 74, 73, and 72 mV/dec, respectively, which smaller than Pt/C, indicating the as-made catalysts have superior electrocatalytic ORR kinetics in alkaline solution.

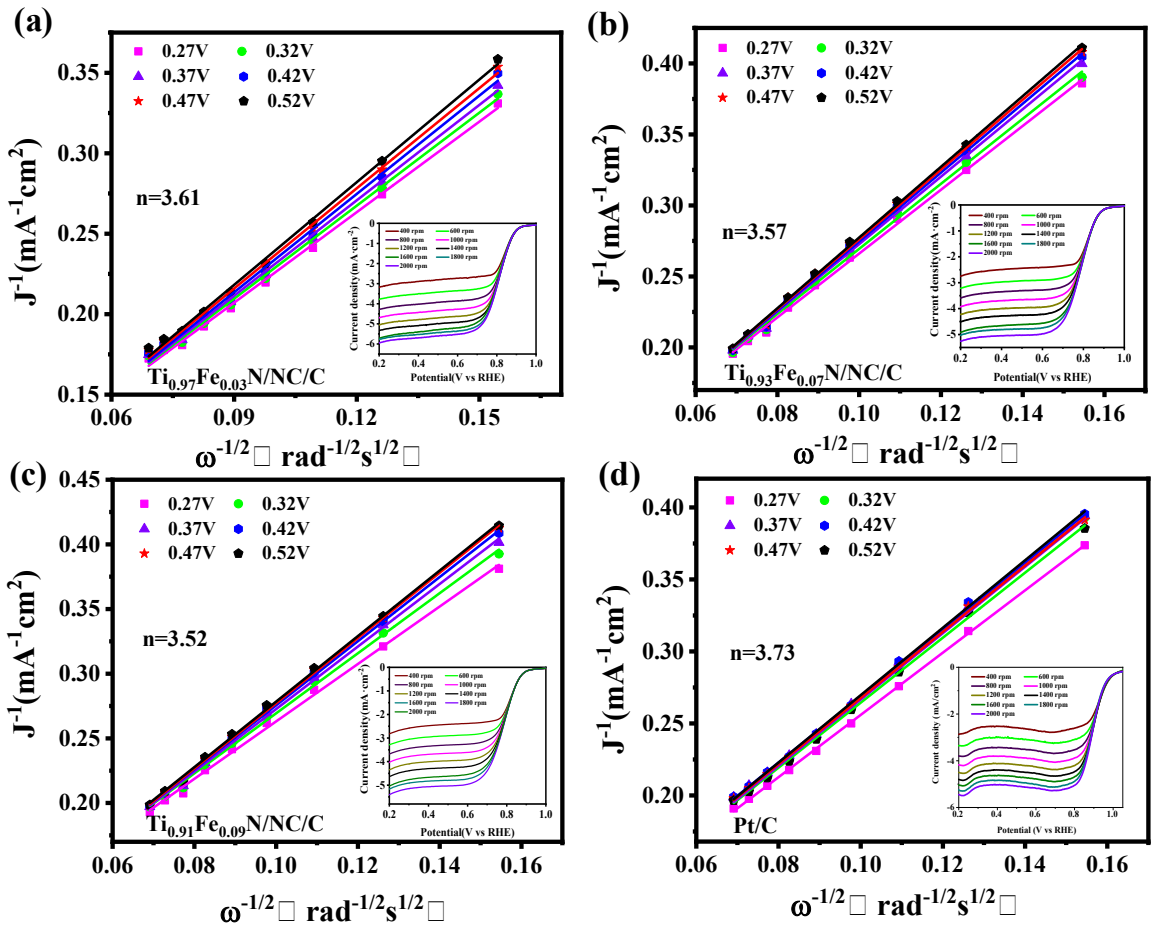


**Figure S7.** K-L plots of the $Ti_{0.97}Fe_{0.03}N/NC/C$, $Ti_{0.93}Fe_{0.07}N/NC/C$, $Ti_{0.91}Fe_{0.09}N/NC/C$ and Pt/C catalysts between potentials 0.27 V and 0.52 V.

Furthermore, the K-L equation was applied to estimate the kinetic progress of $Ti_xFe_{1-x}N/NC/C$ and Pt/C catalysts. From the fitted data between the potentials 0.27 and 0.52 V, the K-L plots shows approximate linearity and closed slops. The corresponding average electron transfer numbers are 3.61, 3.57, 3.52 and 3.73, respectively. The results demonstrate that the electron transfer number of as-made catalysts is dominated by 4 electrons, which is close to Pt/C, showing that iron doping improves catalytic activity.

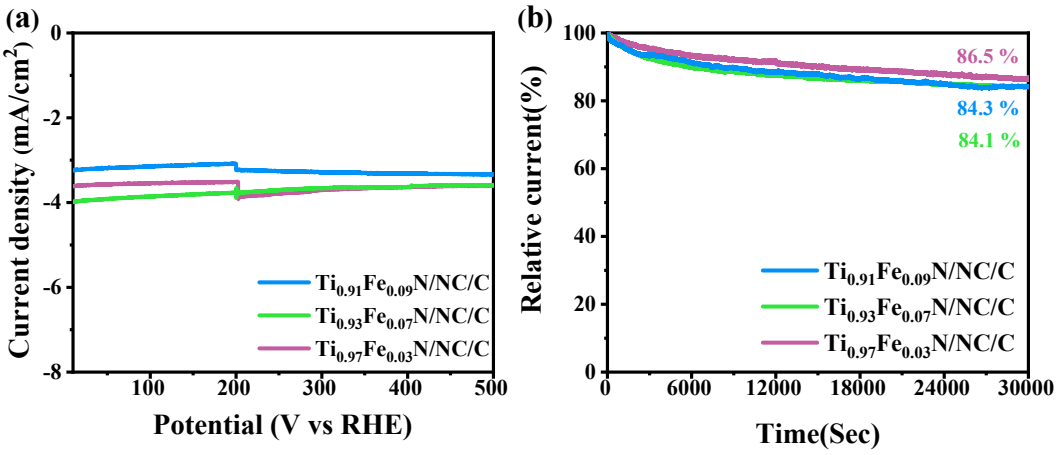


**Figure S8.** (a) Effect of 3 M methanol on the ORR activity of $Ti_{0.97}Fe_{0.03}N/NC/C$, $Ti_{0.93}Fe_{0.07}N/NC/C$ and $Ti_{0.91}Fe_{0.09}N/NC/C$ in $O_2$-saturated 0.1 M KOH electrolyte. (b) ORR i-t plots of the $Ti_{0.97}Fe_{0.03}N/NC/C$, $Ti_{0.93}Fe_{0.07}N/NC/C$ and $Ti_{0.91}Fe_{0.09}N/NC/C$.

The methanol resistance was measured by chronoamperometry in an $O_2$-saturated 0.1 M KOH solution. Introducing 3M methanol into the electrolyte at 200 s, the current density of $Ti_xFe_{1-x}N/NC/C$ had no alteration, proving that the as-made catalysts have an excellent methanol tolerance. Moreover, chronoamperometry measurement is also used for testing the durability of the catalysts. after 30000 s of measurement, the $Ti_{0.91}Fe_{0.09}N/NC/C$, $Ti_{0.93}Fe_{0.07}N/NC/C$, and $Ti_{0.97}Fe_{0.03}N/NC/C$ catalysts hold about 84.3%, 84.1% and 86.5% of the initial current, respectively. The as-prepared catalysts are more stable than Pt/C and have a considerable chance of replacing commercial noble metal-based catalysts.

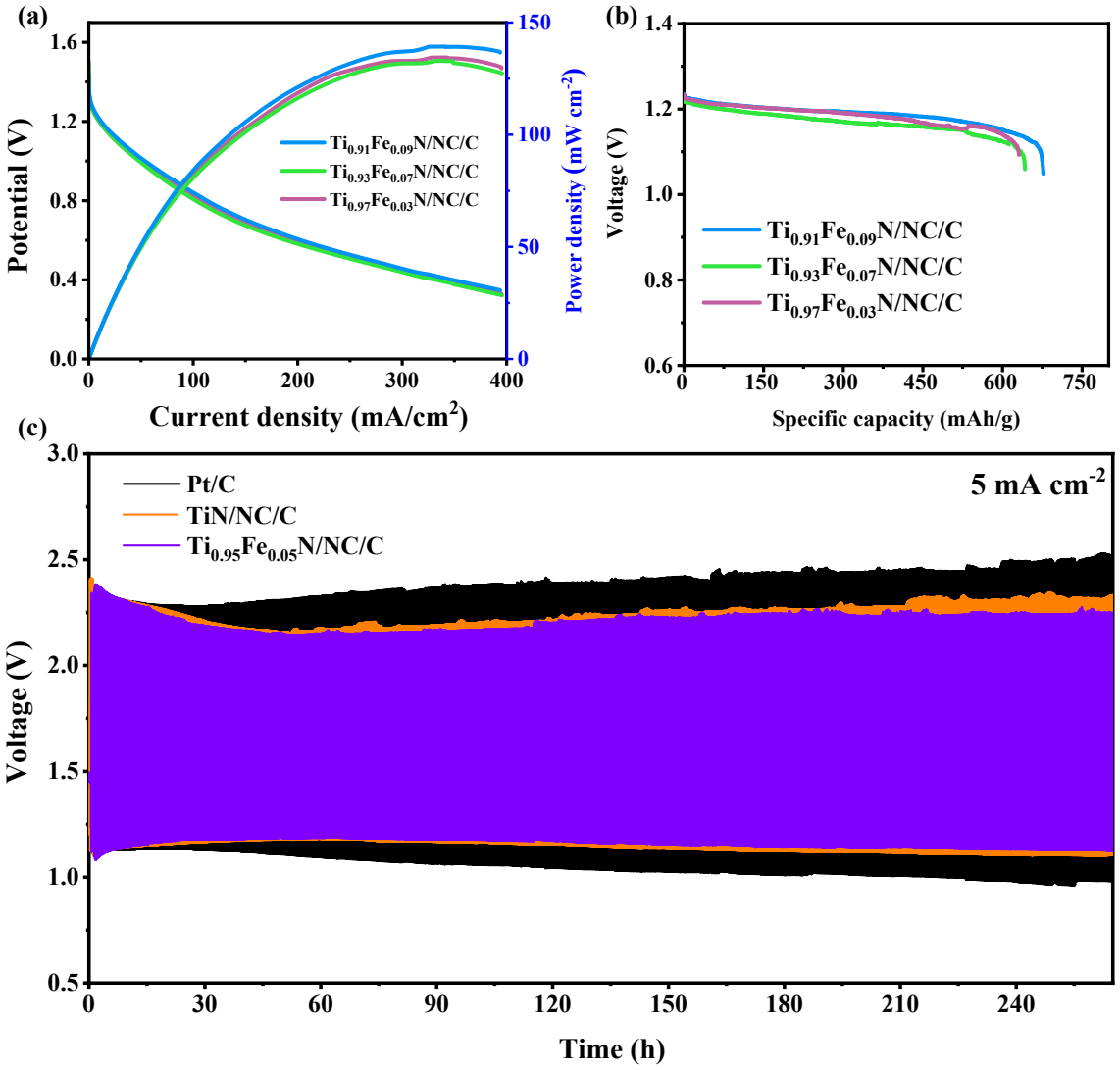


**Figure S9.** (a) Polarization curves and the corresponding power density curves of the Zn-air batteries, (b) Specific capacities of the Zn-air batteries based on $Ti_{0.97}Fe_{0.03}N/NC/C$, $Ti_{0.93}Fe_{0.07}N/NC/C$ and $Ti_{0.91}Fe_{0.09}N/NC/C$ as ORR catalysts, respectively. (c) Long-term cycling charge-discharge curve of the TiN/NC/C, $Ti_{0.97}Fe_{0.03}N/NC/C$, and Pt/C catalysts based Zn-air batteries.

As depicted by Figure S8a, the Zn-air batteries equipped with $Ti_{0.91}Fe_{0.09}N/NC/C$, $Ti_{0.93}Fe_{0.07}N/NC/C$, and $Ti_{0.97}Fe_{0.03}N/NC/C$ catalysts exhibit a prominent peak power density of 139.1 $mA \cdot cm^{-2}$, 132.7 $mA \cdot cm^{-2}$, 134.9 $mA \cdot cm^{-2}$, respectively, which is similar to the Pt/C-based

catalyst. Furthermore, the discharge polarization curves are shown in the Figure S8b. At the discharge current density of 10 $mA \cdot cm^{-2}$, the Zn-air battery based on $Ti_{0.97}Fe_{0.03}N/NC/C$, $Ti_{0.93}Fe_{0.07}N/NC/C$ and $Ti_{0.91}Fe_{0.09}N/NC/C$ have specific capacities and energy densities of 630.6 $mAh \cdot g_{zn}^{-1}$ and 751.1 $Wh \cdot kg_{zn}^{-1}$, 640.8 $mAh \cdot g_{zn}^{-1}$ and 747.5 $Wh \cdot kg_{zn}^{-1}$, 675.2 $mAh \cdot g_{zn}^{-1}$ and 793.7 $Wh \cdot kg_{zn}^{-1}$, respectively.

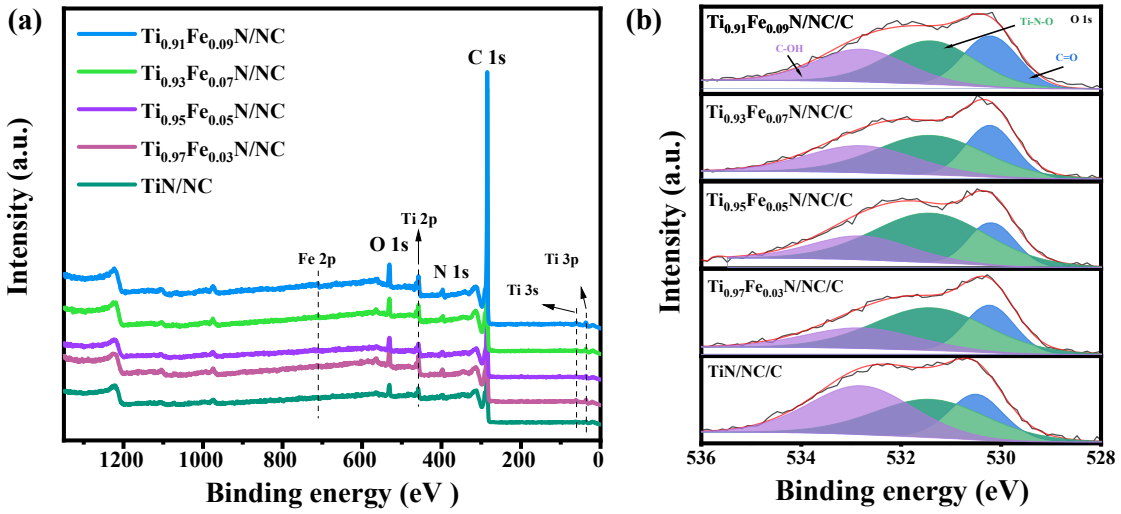


**Figure S10.** (a) XPS survey spectrum. (b) The O 1s high-resolution XPS spectrum of the TiN/NC/C, $Ti_{0.97}Fe_{0.03}N/NC/C$, $Ti_{0.93}Fe_{0.07}N/NC/C$, $Ti_{0.95}Fe_{0.05}N/NC/C$ and $Ti_{0.91}Fe_{0.09}N/NC/C$ composite.

The survey spectrum shown in Figure S9a reveals that the as-prepared composite contains C, N, O, Ti and Fe elements. The O 1s high-resolution spectrum contains three peaks as shown in the Figure S9b. The peak at 530.5 and 532.8 eV assigned to the C=O and C-OH, respectively. The peak located at 531.4 eV corresponds to the Ti-N-O, illustrating partial oxidation of TiN surface.

**Table S1.** ORR performance parameters of as-prepared catalysts.

| Catalysts | $E_{oneset}$ (V) | $E_{1/2}$ (V) | $[J_L]$ (mA·cm$^{-2}$) |
|---|---|---|---|
| **TiN/NC/C** | 0.78 | 0.70 | 4.35 |
| **$Ti_{0.97}Fe_{0.03}$N/NC/C** | 0.89 | 0.82 | 5.81 |
| **$Ti_{0.95}Fe_{0.05}$N/NC/C** | 0.89 | 0.83 | 5.96 |
| **$Ti_{0.93}Fe_{0.07}$N/NC/C** | 0.88 | 0.82 | 5.25 |
| **$Ti_{0.91}Fe_{0.09}$N/NC/C** | 0.88 | 0.82 | 5.07 |
| **Pt/C** | 0.96 | 0.90 | 5.15 |

**Table S2.** Surface compositions of the $Ti_xFe_{1-x}$N/NC/C catalysts by XPS.

| Catalysts | C 1s (at.%) | N 1s (at.%) | O 1s (at.%) | Ti 2p (at.%) | Fe 2p (at.%) |
|---|---|---|---|---|---|
| **TiN/NC/C** | 93.90 | 1.03 | 3.97 | 1.10 | —— |
| **$Ti_{0.97}Fe_{0.03}$N/NC/C** | 89.73 | 3.46 | 5.11 | 1.55 | 0.15 |
| **$Ti_{0.95}Fe_{0.05}$N/NC/C** | 89.25 | 3.03 | 6.55 | 1.03 | 0.14 |
| **$Ti_{0.93}Fe_{0.07}$N/NC/C** | 90.54 | 1.04 | 7.23 | 1.02 | 0.17 |
| **$Ti_{0.91}Fe_{0.09}$N/NC/** | 88.75 | 1.36 | 8.30 | 1.37 | 0.22 |

| | |
|---|---|
| **C** | |

**Table S3.** Carbon species in the $Ti_xFe_{1-x}N/NC/C$ catalysts determined by XPS using C 1s.

| Catalysts | C-C/C=C (at.%) | C-C (at.%) | C-N/C-O (at.%) | C=N/C=O (at.%) |
|---|---|---|---|---|
| **TiN/NC/C** | 4.41 | 81.34 | 10.42 | 3.54 |
| **$Ti_{0.97}Fe_{0.03}N$/NC/C** | 3.92 | 76.63 | 14.97 | 4.48 |
| **$Ti_{0.95}Fe_{0.05}N$/NC/C** | 4.39 | 76.58 | 15.76 | 3.27 |
| **$Ti_{0.93}Fe_{0.07}N$/NC/C** | 4.55 | 80.53 | 12.59 | 2.32 |
| **$Ti_{0.91}Fe_{0.09}N$/NC/C** | 3.99 | 77.98 | 14.62 | 3.41 |

**Table S4.** Nitrogen species in the $Ti_xFe_{1-x}N/NC/C$ catalysts determined by XPS using N 1s.

| Catalysts | Ti-N-O (at.%) | Ti-N (at.%) | pyridinic-N (at.%) | pyrrolic-N (at.%) | graphitic-N (at.%) | Oxidized-N (at.%) |
|---|---|---|---|---|---|---|

| | | | | | | |
|---|---|---|---|---|---|---|
| **TiN/NC/C** | 8.05 | 8.92 | 1.91 | 18.43 | 43.26 | 19.43 |
| **$Ti_{0.97}Fe_{0.03}$N/NC/C** | 8.85 | 51.47 | 21.05 | 8.13 | 6.28 | 4.22 |
| **$Ti_{0.95}Fe_{0.05}$N/NC/C** | 26.58 | 13.47 | 20.06 | 5.66 | 28.6 | 5.63 |
| **$Ti_{0.93}Fe_{0.07}$N/NC/C** | 34.75 | 14.77 | 15.46 | 11.67 | 21.48 | 1.87 |
| **$Ti_{0.91}Fe_{0.09}$N/NC/C** | 29.84 | 18.28 | 20.08 | 4.17 | 22.54 | 5.09 |

**Table S5.** Titanium species in the $Ti_xFe_{1-x}N$/NC/C catalysts determined by XPS using Ti 2p.

| **Catalysts** | **Ti-N/O (at.%)** | **Ti-O (Ti $2p_{3/2}$) (at.%)** | **Ti-N (at.%)** | **Ti-O (Ti $2p_{1/2}$) (at.%)** |
|---|---|---|---|---|
| **TiN/NC/C** | 15.31 | 53.35 | 3.31 | 28.03 |
| **$Ti_{0.97}Fe_{0.03}$N/NC/C** | 31.34 | 35.72 | 14.23 | 18.71 |
| **$Ti_{0.95}Fe_{0.05}$N/NC/** | 31.54 | 32.88 | 18.06 | 17.52 |

| | | | | |
|---|---|---|---|---|
| **C** | | | | |
| **$Ti_{0.93}Fe_{0.07}N$/NC/C** | 29.12 | 34.53 | 18.90 | 17.45 |
| **$Ti_{0.91}Fe_{0.09}N$/NC/C** | 31.36 | 34.52 | 18.06 | 16.06 |

**Table S6.** Iron species in the $Ti_xFe_{1-x}N$/NC/C catalysts determined by XPS using Fe 2p.

| Catalysts | $Fe^{2+}$ $2p_{3/2}$ (at.%) | $Fe^{3+}$ $2p_{3/2}$ (at.%) | $Fe^{2+}$ $2p_{1/2}$ (at.%) | $Fe^{3+}$ $2p_{1/2}$ (at.%) | Satellite (at.%) |
|---|---|---|---|---|---|
| **$Ti_{0.97}Fe_{0.03}N$/NC/C** | 33.61 | 24.34 | 6.31 | 21.08 | 14.65 |
| **$Ti_{0.95}Fe_{0.05}N$/NC/C** | 28.32 | 24.74 | 7.77 | 20.98 | 18.19 |
| **$Ti_{0.93}Fe_{0.07}N$/NC/C** | 21.69 | 47.1 | 2.25 | 20.04 | 8.91 |
| **$Ti_{0.91}Fe_{0.09}N$/NC/C** | 39.09 | 20.00 | 4.48 | 22.95 | 13.47 |

## Reference


1. Z. F. Huang, J. Wang, Y. C. Peng, C. Y. Jung, A. Fisher and X. Wang, Design of Efficient Bifunctional Oxygen Reduction/Evolution Electrocatalyst: Recent Advances and Perspectives, Adv. Energy Mater., 2017, **7**, 21.
2. C. L. Li, M. C. Wu and R. Liu, High-performance bifunctional oxygen electrocatalysts for zinc-air batteries over mesoporous Fe/Co-N-C nanofibers with embedding FeCo alloy nanoparticles, Appl. Catal. B-Environ., 2019, **244**, 150-158.
3. Y. L. Liu, Y. S. Shen, S. M. Zhu and D. Y. Li, TiN nanoparticles hybridized with Fe, N co-doped carbon nanosheets composites as highly efficient electrocatalyst for oxygen reduction reaction, *Chem. Eng. J.*, 2020, **400**, 8.
4. X. L. Tian, L. J. Wang, B. Chi, Y. Y. Xu, S. Zaman, K. Qi, H. F. Liu, S. J. Liao and B. Y. Xia, Formation of a Tubular Assembly by Ultrathin Ti0.8Co0.2N Nanosheets as Efficient Oxygen Reduction Electrocatalysts for Hydrogen-/Metal-Air Fuel Cells, ACS Catal., 2018, **8**, 8970-8975.
5. Y. L. Zhao, Y. H. Wang, L. Dong, Y. Zhang, J. J. Huang, J. B. Zang, J. Lu and X. P. Xu, Core-shell structural nanodiamond@TiN supported Pt nanoparticles as a highly efficient and stable electrocatalyst for direct methanol fuel cells, Electrochimica Acta, 2014, 148, **8**-14.
6. X. L. Tian, J. M. Luo, H. X. Nan, H. B. Zou, R. Chen, T. Shu, X. H. Li, Y. W. Li, H. Y. Song, S. J. Liao and R. R. Adzic, Transition Metal Nitride Coated with Atomic Layers of Pt as a Low-Cost, Highly Stable Electrocatalyst for the Oxygen Reduction Reaction, *Journal of the American Chemical Society*, 2016, **138**, 1575-1583.